

Field-ionization rates of the hydrogen molecular ion

To cite this article: M Plummer and J F McCann 1996 *J. Phys. B: At. Mol. Opt. Phys.* **29** 4625

View the [article online](#) for updates and enhancements.

You may also like

- [Generation and coherent control of even-order harmonics driven by intense frequency-comb and cavity-mode fields inside a fsEC](#)

Di Zhao, Fu-li Li and Shih-I Chu

- [High-frequency approximation for periodically driven quantum systems from a Floquet-space perspective](#)

André Eckardt and Egidijus Anisimovas

- [Controlling stable tunneling in a non-Hermitian spin-orbit coupled bosonic junction](#)

Yunrong Luo, Xuemei Wang, Yuxin Luo et al.



Easy-to-use and Helium-3 free
cryogenics solutions

LEARN MORE

Field-ionization rates of the hydrogen molecular ion

M Plummer and J F McCann

Atomic and Molecular Physics Group[†], Department of Physics, University of Durham, Durham DH1 3LE, UK

Received 22 May 1996

Abstract. We calculate the quasienergies and wavefunctions of the hydrogen molecular ion perturbed by a strong external electric field. Results are obtained for static-field ionization rates of the lowest dressed states. The nonlinear Stark shifts are also calculated for weak and strong fields for a range of internuclear separations. Charge and current densities are obtained and used to explain the ionization resonance structure. The ionization currents are found to be very sensitive to field strength and internuclear distance. There is evidence of critical distances that indicate the validity of Coulomb explosion models and electron localization. However, for this system, the results do not agree well with simple over-barrier models of electron release. Multiphoton ionization rates of low-frequency intense laser fields are estimated by cycle averaging.

1. Introduction

Dissociative ionization of diatomic molecules by a low-frequency intense laser is a subject of current interest. The recent progress in this field has been adequately reviewed in the following papers: Codling and Frasinski (1993), Schmidt *et al* (1994) and Giusti-Suzor *et al* (1995). The ionization of atoms or molecules by intense laser fields is usually a complicated nonperturbative tug-of-war between the internal and external fields, and poses many experimental and theoretical difficulties. In particular, the high degree of fragmentation is a persistent problem. One of the questions that remain to be answered is the sequence and nature of this fragmentation. However, important experimental work using a covariance-mapping method has greatly illuminated the important physical processes (Codling and Frasinski 1993).

The gross features of the multiple ionization and dissociation of heavy systems, such as the iodine dimer, seem to be well reproduced by the Coulomb explosion model (Posthumus *et al* 1995). For a variety of laser intensities and ionization fractions the following observation was made. The kinetic energy of the ions appears to be an approximately constant fraction of the electrostatic (Coulomb) energy of the ions at the molecular equilibrium distance R_E . Thus for a homonuclear diatomic molecule which fragments into the ions X^{p+} , X^{q+} , the energy released is given approximately by $f p q e^2 / (4\pi\epsilon_0 R_E)$ with $0 \leq f \leq 1$ dependent only on the original molecular equilibrium distance R_E .

Possible explanations for these results might lie in either the stabilization of the molecule in the field, or in terms of enhanced tunnel ionization. In the first case the molecular ion, in a low degree of ionization, expands to a distance $R_D > R_E$ at which a stable ('trapped') field-molecule state is formed. Additional ionization then occurs around R_D and the ion kinetic

[†] <http://www.dur.ac.uk/~dph0www1>

energy is simply given by $pqe^2/(4\pi\epsilon_0 R_D)$. Stabilization has been predicted theoretically in models of H_2^+ dissociation (Plummer and McCann 1995a) and for H_3^{2+} (Zuo and Bandrauk 1995a) in high-frequency fields but does not seem a realistic mechanism for highly charged molecular ions. The second hypothesis has the molecule dissociating to a distance R_D at which the tunnel ionization rate for successive electrons is strongly peaked: the ionization is assumed to occur very quickly compared to the optical cycle time and vibrational period. The Coulomb explosions thus all occur from this distance R_D . At small values of the Keldysh parameter, corresponding to low optical frequencies and high laser intensities, tunnelling is the dominant mechanism for ionization. Atomic ionization rates based upon cycle-averaged static-field rates compare very well with detailed dynamic field calculations (Dörr *et al* 1990). The same mechanism should also apply to molecular photoionization and one would expect studies of static field ionization of molecules to yield useful insights regarding the behaviour of molecules in low-frequency dynamic fields.

This second interpretation has recently been investigated quantitatively and several papers have developed the argument. Posthumus *et al* (1995), Seideman *et al* (1995) and Chelkowski and Bandrauk (1995) develop semiclassical models for fragmentation of many-electron diatomic molecules which aid the interpretation of the experimental data. Zuo and Bandrauk (1995b) consider the ionization of H_2^+ in an intense 1064 nm laser field parallel to the internuclear axis at various values of R by numerical solution of the time-dependent Schrödinger equation. They find a high ionization rate at large R (between $6 a_0$ and $12 a_0$) which exceeds the atom limit by at least an order of magnitude. Chelkowski *et al* (1995) perform a three-body calculation of dissociative ionization of H_2^+ in a 212 nm field and also find high ionization rates at large R .

In the absence of the field and for internuclear distances beyond several Bohr radii, a molecule will revert to its atomic constituents. For the system H_2^+ the bound eigenstates will be localized, though slightly polarized, hydrogen orbitals. As is well known, an external electric field along the molecular axis will perturb the reflection symmetry of the potential. Thus the separated-atom-limit degeneracy of the lowest two field-free electronic states, of Σ_g^+ and Σ_u^+ symmetry, respectively, is removed. The splitting of the states for large R is approximately the dipole energy eFR with F the field strength (this is demonstrated in figure 1(a) of section 3). Though the reflection symmetry is broken by the external field, we can still retain the labels g and u (meaning, for example, 'ground' and 'upper') to describe the two lowest dressed states of the system. Even for large external fields, the molecular binding of the g-state near equilibrium separation is sufficient to embed this state firmly in the potential well. The antibonding (u) orbital, on the other hand, is nearer the continuum, has a higher ionization rate and is easily distorted as we shall see.

The multiphoton ionization process for fixed nuclei using high-frequency fields has been analysed within the Floquet framework in an earlier paper (Plummer and McCann 1995b, hereafter referred to as I). At certain values of R , resonant enhancement of ionization was predicted. In the present paper we consider the low-frequency case in some detail, using the same theoretical framework. We compare field ionization rates for H_2^+ with results of Ivanov (1995) and Zuo and Bandrauk (1995b) and we calculate cycle-averaged ionization rates applicable to longer wavelengths such as 1064 nm for laser intensities in the range around $10^{14} \text{ W cm}^{-2}$. Finally, we note that molecular field ionization has applications in other areas, one of which is scanning tunnelling microscopy (STM). Data for the tunnelling currents of atoms or molecules helps in their identification and localization when adsorbed on surfaces.

2. Method of calculation of dressed states

Our calculations use the method of real and complex basis functions described in I, using prolate spheroidal coordinates (λ, μ, ϕ) . The basis functions are of the form

$$\psi_i = N_i \mu^{n_i} e^{-\alpha_i \lambda} \quad (1)$$

with N_i a normalization constant. n_i determines the parity of these functions. In the field-free case the Hamiltonian and overlap matrices are block diagonal with Σ_g^+ (even n_i) and Σ_u^+ (odd n_i) blocks. We use basis 4 of I for the α_i : a set of 16 real parameters augmented by six complex parameters obtained by rotating the smaller α_i into the lower half-plane. These α_i then give trial functions with the appropriate diverging wave character. All the trial functions are square-integrable and matrix elements are formed straightforwardly, using analytic continuation where required. This mixture of real and complex functions mimics a rotation or complex scaling of the Hamiltonian coordinates and allows us to obtain converged results for strong fields, with a moderate number of functions. Further details and discussion are given in I.

The current calculations are essentially the same as the length-gauge Floquet calculations of I, but with one diagonal block for each symmetry and one off-diagonal dipole symmetry-mixing block. The Σ_g^+ and Σ_u^+ functions are mixed by the field, though the axial symmetry means that the two lowest dressed states have Σ^+ symmetry. In this case we require larger blocks for convergence than in I: we need spheroidal angular functions with $n_i \leq 10$ for Σ_g^+ and $n_i \leq 11$ for Σ_u^+ symmetry. This reflects the fact that the external field produces a strong anisotropy in the system. The complex-symmetric Hamiltonian matrix is then formed with no complex conjugation of the complex α_i , and complex eigenvalues and eigenfunctions are found. The eigenvalues are the quasienergies of the system and can be separated into real and imaginary parts according to

$$E = E_R - i\Gamma/2 \quad (2)$$

with E_R corresponding to the shifted energy and Γ the ionization rate of the state, using atomic units. The eigenfunctions are dressed states of the molecule under the effect of the external perturbation.

We consider the example of a field aligned along the molecular axis. The method can be used for any orientation, but this is the simplest and most physically important case (Codling and Frasinski 1993). Taking the origin at the internuclear midpoint the Hamiltonian is of the form:

$$\begin{aligned} H &= -\frac{1}{2}\nabla^2 - \frac{4\lambda}{R(\lambda^2 - \mu^2)} + \frac{1}{2}RF\lambda\mu \\ &= -\frac{1}{2}\nabla^2 - \frac{1}{((z - \frac{1}{2}R)^2 + \rho^2)^{1/2}} - \frac{1}{((z + \frac{1}{2}R)^2 + \rho^2)^{1/2}} + Fz \end{aligned} \quad (3)$$

in prolate spheroidal coordinates and cylindrical coordinates, respectively. The use of complex eigenvalues to give lifetimes for atomic systems in external fields is discussed by Maquet *et al* (1983).

We have tested our calculations for stability with respect to our basis set, and can confirm the accuracy of the results presented, with the possible exceptions of calculations at both very large R and high F for which our results are not fully converged. We point out these exceptions as we discuss them in the next section. The choice of rotation angle parameter for the complex α_i , and the number of basis functions were the principal considerations. In previous high-frequency multiphoton-ionization rate calculations, the length gauge H_2^+ calculations with many Floquet blocks were not as stable as the corresponding velocity

gauge calculations (I). Fortunately the DC calculations are quite stable for field strengths up to $F = 0.1$ au. When the ionization rates are extremely small as is the case for very weak fields or tightly bound states, there are numerical difficulties using our method; the precise nature of the problem is discussed in I. For example, ionization rates for the g-state at small R and low-field strengths are very small. Nonetheless, comparing our results with those of Ivanov (1995): we have very good agreement for the shifted real energies for all R and good agreement for the ionization rate when $\Gamma \geq 10^{-10}$ au.

We can examine other physical effects of interest. In particular, the charge and current distributions can be calculated using this method. The wavefunctions are square-integrable representations of resonance-like continuum wavefunctions and will be accurate over a finite region of configuration space (Reinhardt 1979, Broad 1982). We must consider possible distortions of our wavefunctions due to their square-integrable nature. To compare wavefunctions calculated at different values of R we also need to consider the correct method of normalization. Watson (1986) discusses the normalization of resonance wavefunctions. Potvliege and Shakeshaft (1989) discuss normalization of Floquet wavefunctions, and Piraux and Shakeshaft (1994) discuss the interpretation of the norm of wavefunctions obtained using the complex-scaling method.

We have constructed wavefunctions normalized in two ways, using $\langle \Psi | \Psi \rangle = 1$ and $\langle \Psi^* | \Psi \rangle = 1$ (i.e. without complex conjugation of the α_i), with integration over spatial coordinates. The second case corresponds to an overlap integral between the wavefunction and its time-reversed counterpart and is consistent with our complex-symmetric method of solution: eigenstates are orthonormal with respect to this form of overlap. This norm is also time independent if the exponential time-dependent factors are included in the two wavefunctions. The complex-conjugated norm decays as $e^{-\Gamma t}$. As discussed by Watson (1986), the (spatially) complex-symmetric normalization is correct for resonance wavefunctions, although for exact wavefunctions the radial integration must be taken to a finite limit beyond which the wavefunctions have their asymptotic form, and a correction term then added. Potvliege and Shakeshaft (1989) discuss the use of the overlap between a Floquet wavefunction and its time-reversed counterpart to give a time-independent normalization.

Piraux and Shakeshaft (1994) consider the general time-dependent atomic wavefunction propagated in the presence of a sinusoidal AC field. They note that the norm defined by the overlap of the wavefunction with its time-reversed counterpart is time independent, and consider the standard norm (with complex conjugation) in detail. For the exact wavefunction this norm is preserved over time; however, for approximate wavefunctions expanded on a finite basis there are problems. If the basis functions are real, the norm is preserved. This means that if the basis is adequate over a sphere of radius r_{\max} in configuration space, and thus cannot represent the probability density outside the sphere, then the preserved norm implies unphysical reflection of the wavefunction back into the sphere. With a complex basis, if the norm is taken over a finite volume then it decays in time as the probability density becomes significant outside the sphere. Piraux and Shakeshaft demonstrate that with a large basis of complex radial Sturmian functions, equivalent to complex scaling, the norm taken over all space is not constant in time as the wavefunction propagates. In fact, it does not converge with increasing basis size although convergence can be obtained by reconstruction using Padé approximants.

For our wavefunctions, which are essentially metastable states in the (strong) DC field, we conclude that the complex-symmetric normalization is correct. In fact, for the g-states there is little discernable difference where probability density is significant (below $\sim 0.05\%$ for $F = 0.0534$ au, rising to between ~ 2 and $\sim 5\%$ for $F = 0.08$ au), between

wavefunctions with the two normalizations. In the case of the upper state there is some difference between the two wavefunctions when the ionization rate is high. Using the complex-symmetric normalization, there is a residual component such that the normalized function $|\Psi|^2$ does not decay rapidly at large distances from the nuclei in directions with falling potential energy. For example, this function falls to between 10^{-8} – 10^{-10} au for $R = 9 a_0$ and $F = 0.0534$ au. This residual component is negligible in comparison with the features of interest in the region surrounding the nuclei. It may be interpreted as partly due to reflected flux (Piroux and Shakeshaft 1994) but it seems reasonable to attribute it mainly to the non-decaying continuum. In such circumstances the densities obtained with the complex-conjugated normalization are smaller than those with the complex-symmetric normalization. However, the difference is usually less than 5%, becoming slightly higher around ionization maxima. The only exception is for the highest field strength considered ($F = 0.08$ au), described in the next section. On the logarithmic scales we use there is again little difference between the two normalizations. This is encouraging and hopefully indicates we have good physical representation of the system. This also allows us to construct the probability current which requires the standard definition of probability density.

3. Results and discussion

In figure 1 the energy and ionization rates for the lower (g) and upper (u) dressed states are given for various R , and for different field strengths. We note the conversion from field strength (F in atomic units) to equivalent laser peak intensity (I in W cm^{-2}) is given by $F \approx 5.338 \times 10^{-9} \sqrt{I}$. As expected the g rates are much lower than the u rates except at very high field strengths, and show a gradual increase as R increases and the molecular effect is reduced. For very high fields there is some oscillation in the rates with R . The u-state rates have more interesting features. At lower field strengths ($F \leq 0.04$ au) there are two maxima, the second larger than the first, as R increases. These maxima shift to lower R , and are greatly amplified, as the field strength is increased. In the higher fields a set of oscillations develops after the large maximum.

Only some of the maxima in the u-state rates can be explained using the potential-barrier model (Codling and Frasinski 1993, Posthumus *et al* 1995, Zuo and Bandrauk 1995b, Chelkowski and Bandrauk 1995). In this classical model ionization is controlled by the height of the potential barriers with respect to the electronic energy. Ionization is enhanced when the electric field and ion field act in unison to lower the barrier of the upper well, while the lower well is less favoured because the ion field opposes the tunnelling motion of the electron. Electron release is suppressed when the energy of the electron falls below a potential barrier. An example is given for $F = 0.04$ au in figure 2(a) where the left-hand barrier ($z < 0$) and middle barrier impede the electron release. Comparing with figure 1(c), the maximum at $R = 7 a_0$ could be attributed to the lowering of the left-hand barrier with respect to the real part of the u-state quasienergy as R increases. For larger R the u-state experiences substantial reflection from the rising and widening middle barrier, and the rate decreases. However, the barrier model does not explain the larger maximum at $R = 11 a_0$: according to the model the rate should be converging to the atomic limit. Figure 2(b) shows a similar set of pictures for $F = 0.05338$ au. The maximum at $R = 5.6 a_0$ can be explained using the barrier model but the minimum at $R = 7.2 a_0$, the large maximum at $R = 9 a_0$ and the subsequent behaviour cannot be so explained. This pattern is repeated for the other field strengths with the maxima shifting to smaller R as F increases. These shifts can be attributed to the steeper potential gradient, consistent with the barrier model.

To find out what is happening at the large maxima we can examine the wavefunctions

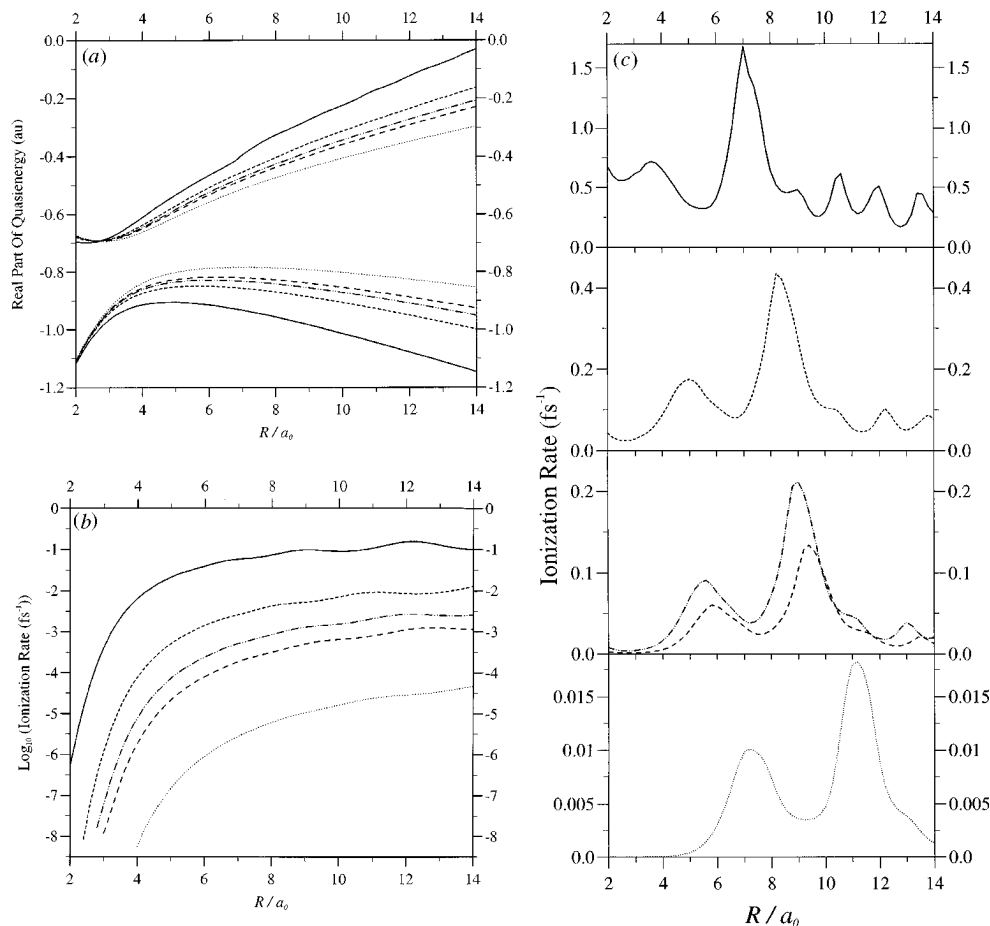


Figure 1. The real parts of quasienergies and ionization rates for varying R at the following field strengths: \cdots , $F = 0.04$ au; $—$, $F = 0.05$ au; $- \cdot -$, $F = 0.05338$ au; $---$, $F = 0.06$ au; $---$, $F = 0.08$ au. (a) Real parts of quasienergies for g- and u-states, (b) ionization rates for the g-states, (c) ionization rates for the u-states.

associated with the quasienergies. We take the case $F = 0.05338$ au as an example and show how $|\Psi|^2$ varies with cylindrical coordinates ρ and z in figure 3. To check on how to interpret the wavefunctions figure 3(a) shows contour plots of g-states for various R . The electron sits in the lower well as expected: for low R there is some residual molecular character on the logarithmic scale. As R and the ionization rate increase there is greater probability density along the negative z -axis.

Figure 3(b) shows the u-states. The electron sits in the upper well; however, there is some interaction with the lower well and continued probability density along the negative z -axis, showing the electron 'leaking' away. At the first maximum at $R = 5.6 a_0$ this leakage is pronounced, then it dies away as R increases. At the minimum at $R = 7.2 a_0$ we see a three-dimensional effect. At the large maximum at $R = 9 a_0$ this effect is pronounced, with a distinct spur at an angle to the z -axis as well as relatively high probability density (with respect to other R values) along the negative z -axis: figure 3(c) shows a three-dimensional plot for $R = 9 a_0$. This feature is still present at $R = 10$ – $12 a_0$ with the ionization

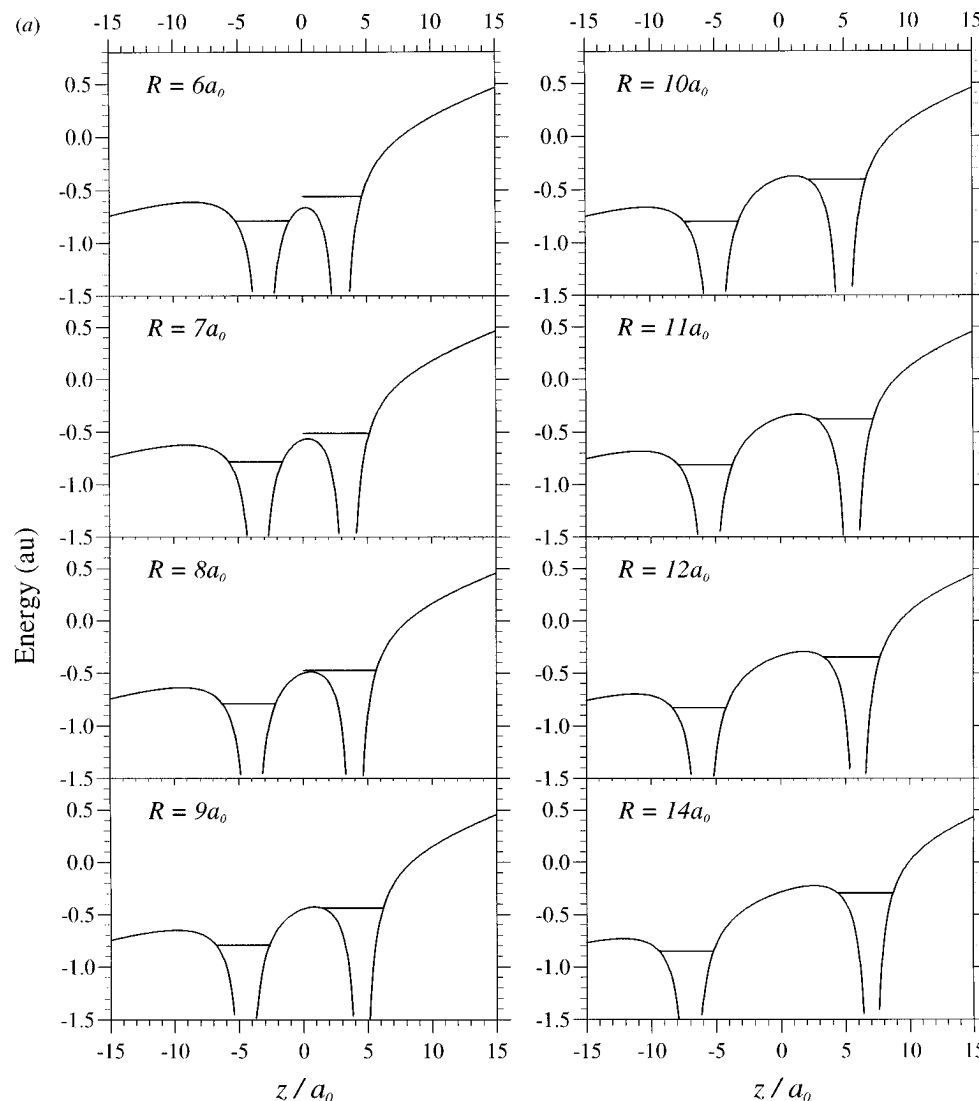


Figure 2. The electronic potential along the internuclear axis for various R , with real parts of g - and u -state quasienergies displayed. (a) $F = 0.04$ au ($R = 6$ – 14 a_0), (b) $F = 0.05338$ au ($R = 4$ – 13 a_0).

rate falling. As R increases, passing through the minimum and reaching a maximum at $R = 13$ a_0 , a third spur develops. Examination of $|\Psi|^2$ for other field strengths shows similar effects at the shifted maxima. We discuss these small oscillations in the large- R ionization rate below, but note that they are not calculated to as high an accuracy as the main features at intermediate and small values of R .

We have examined the probability current density (the real part of $\Psi^* \nabla \Psi$ with standard normalization as noted in section 2). Figure 4 shows the current density for $F = 0.05338$ au at $R = 9$ a_0 . The current in each spur is directed downwards along the spur. At lower R the current for negative z is pointed in a narrow cone about the z -axis. There are more

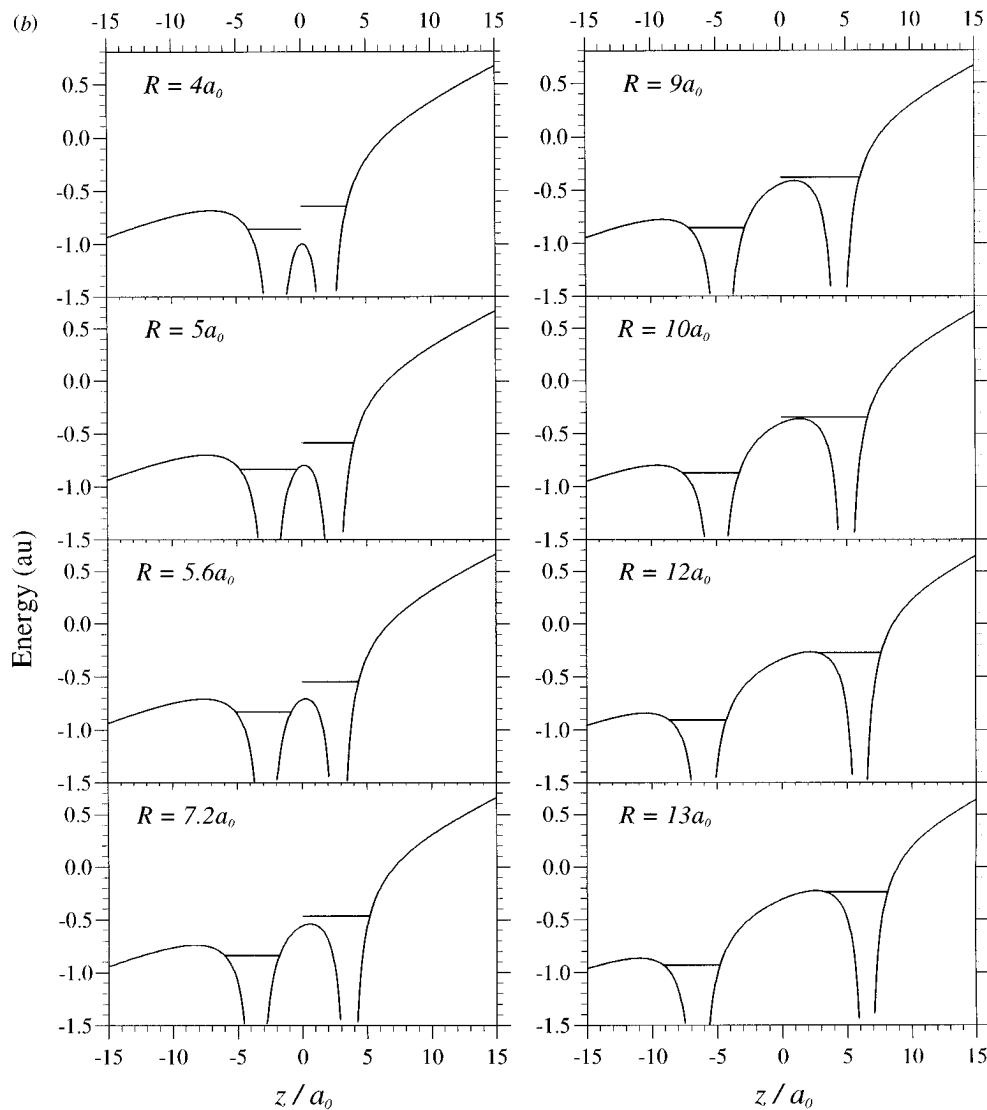


Figure 2. (Continued).

complicated current patterns around the wells, and in the case of figure 4 around the division between the two spurs where $|\Psi|^2$ drops away.

We note the following points concerning the strong field $F = 0.08$ au. At large R the real part of the u quasienergy (figure 1(a)) deviates only slightly from the simple formula, $E = \frac{1}{2}(FR - 1)$, for the energy of a hydrogen atom in a field. However, when the external and ion fields are opposed, corresponding to the g -state, the behaviour is quite different. This is primarily an effect of the long range of the Coulomb field; this asymmetry in the energy shifts does not occur for short-range potentials (McCann and Plummer 1996). The pattern for probability density suggested by the results of figure 3(b) continues for the oscillations in the ionization rate above the large maximum. At $R = 9 a_0$ a third spur is not fully present but a distortion of the two-spur pattern is noticeable. The third spur

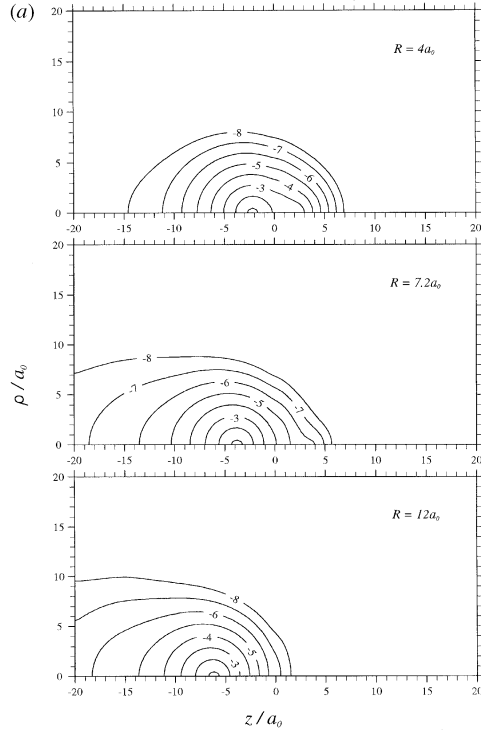


Figure 3. Contour plots of charge density at field strength $F = 0.053\,38$ au. The contours show $\log |\Psi|^2$ at unit intervals, down to -8 . (a) g-state results for $R = 4\text{--}12\,a_0$. (b) u-state results for $R = 4\text{--}13\,a_0$. (c) Three-dimensional plot for the u-state at $R = 9\,a_0$.

develops as R increases and is prominent for the maximum at $R = 10.6\,a_0$. Each successive maximum, as R increases, corresponds to the presence of an additional spur. The u-state rates for this field strength at $R > 10$ au require high powers of μ in the basis set to cope with the reduction in angular symmetry. For this reason our u-state calculations are not fully converged in this region: the pattern of large- R oscillations tends to shift slightly to larger or smaller R as we vary the basis set. However, we believe that they represent an important physical effect (see below). The g-states do not show this unusual behaviour but tend to follow the pattern of figure 3(a).

Figure 5 shows contour plots of both the g- and u-states at $R = 10.6\,a_0$, as well as potentials and (real parts of) quasienergy levels around the large maximum at $R = 7\,a_0$. There is no simple one-dimensional explanation for the large maximum, which as in figure 3(b) has a strong two-spur structure. Three-dimensional effects are extremely important. In the charge density calculation, we note that there is a factor of about 0.3 difference between values of $|\Psi|^2$ obtained with the two normalizations at this maximum: generally for $F = 0.08$ au the factor is above 0.7 for the u-state and above 0.95 for the g-state. For large R , beyond the primary peaks, the small oscillatory peaks are due to potential scattering from the lower well. As the ionized electrons leave the upper well they rescatter from the lower well. The same effect has been noted and investigated in an analysis of electron depletion from quantum-well chains (McCann and Plummer 1996).

Finally, we consider how these results may be adapted to the study of multiphoton ionization (MPI) by dynamic fields. Tables 1 and 2 show time-averaged rates $\bar{\Gamma}$ for the g- and u-states at various R in a sinusoidal field: $F(t) = F_0 \sin(\omega t)$. The average rate is

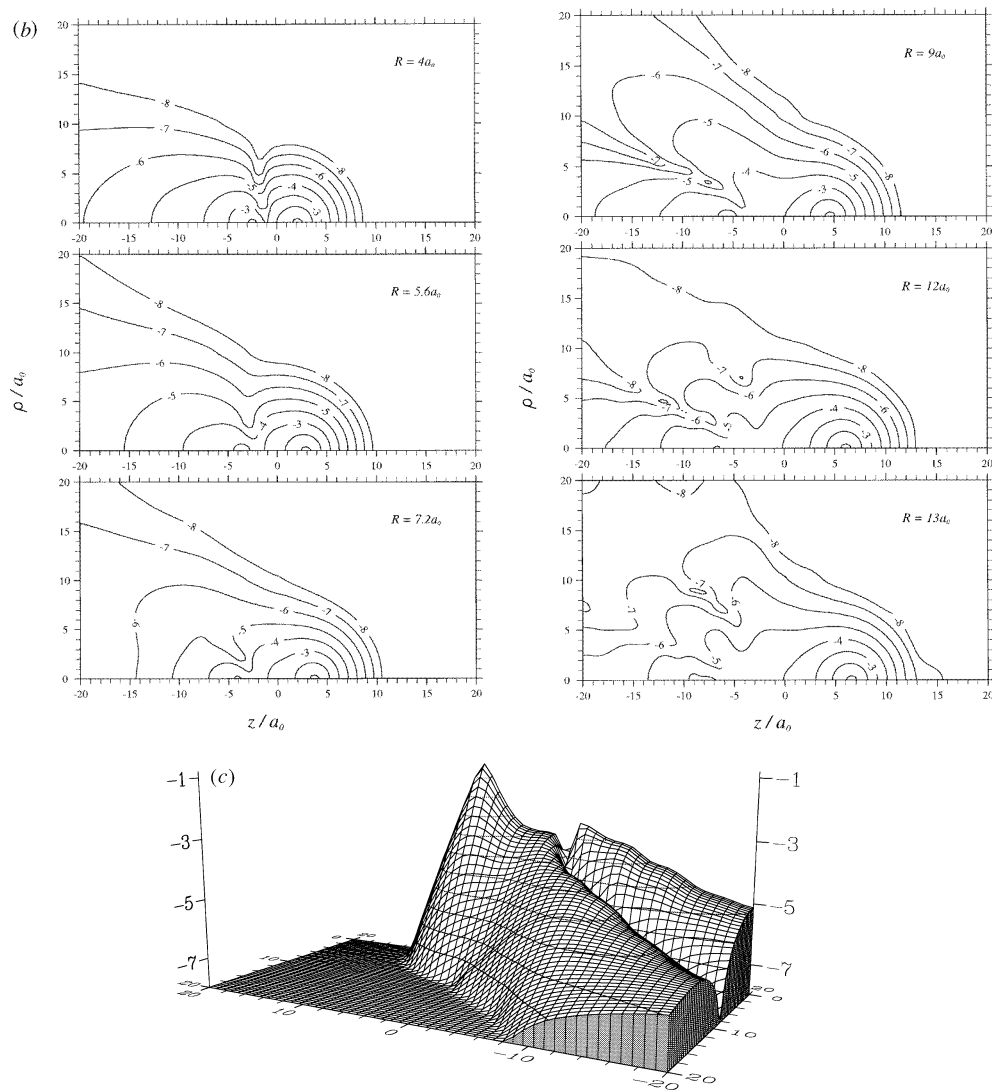


Figure 3. (Continued).

defined as

$$\bar{\Gamma} = \frac{2\omega}{\pi} \int_0^{\pi/2\omega} \Gamma(F) dt \quad (4)$$

where $\Gamma(F)$ is taken as the DC rate for field F . The result for each R and F_0 assumes the g- or u-state changes adiabatically as the field changes and is independent of the AC frequency ω .

Table 1 shows time-averaged results for a sinusoidal field of peak strength $F_0 = 0.05338$ au (equivalent to an intensity of 10^{14} W cm $^{-2}$) and $F_0 = 0.08$ au. Concentrating on the results for $I = 10^{14}$ W cm $^{-2}$, we note that both sets of results follow a similar pattern to the peak-field results of figure 1 as R varies, though the rates are reduced in magnitude. For the g-state this reduction varies from a factor of nearly 6 at low R to just under 5 at

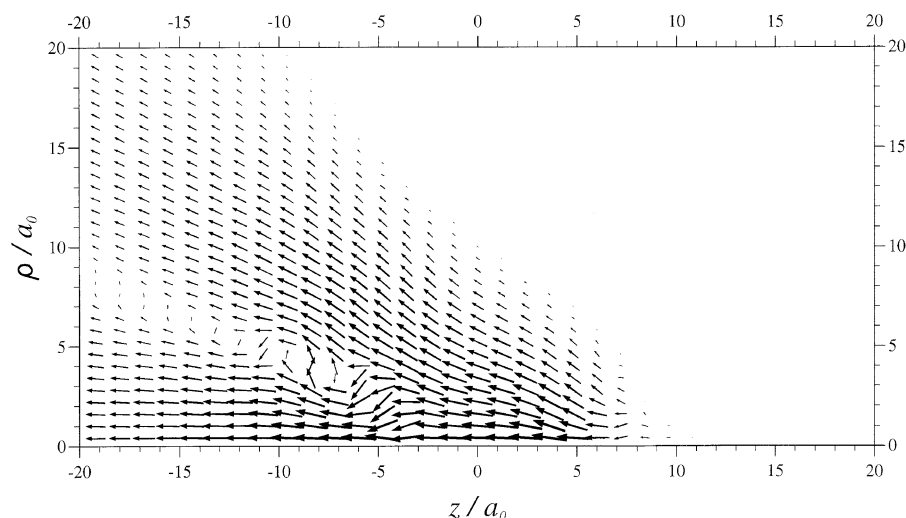


Figure 4. A vector plot of the scaled probability current density for $R = 9 a_0$, $F = 0.053\,38$ au. The magnitude of each vector is given by $\log 10^8 \times \Re(\Psi^* \nabla \Psi)$, with normalization as described in section 2 (atomic units are used).

large R , showing the predominance of the high-field part of the cycle. The time-averaged u-state rates have maxima at the same R -values as the peak-field results, as one would expect from the dramatic rise in ionization probability as the field increases. However, the time-averaged curve does retain the signature of the rising field in that the peaks show a slight enhancement to the right-hand side of the peaks. This is a feature of the ionization maxima occurring at larger R for lower field strengths (figure 1(c)). The smaller maximum at $R = 13 a_0$ is present but to a lesser extent, due to this distortion. The rates are a factor varying from about 5 to 2.5 smaller than the peak field rates. The u-state results are much larger than the g-state rates. Time-averaged results for the other peak fields behave in a similar way, with the maxima shifted very slightly to the right.

Clearly the time-averaged results confirm that population of the u-state is required to explain observed or calculated AC ionization rate variation with R , and to justify the ‘enhanced ionization rate’ explanation of the nuclear Coulomb explosion. A molecule for which the electronic state varies adiabatically from the field-free g-state would not have this variation in ionization rate, and calculations using only the g-state would have to demonstrate the occurrence of trapping.

We may also compare time-averaged results for the u-state with figure 1 of Zuo and Bandrauk (1995b), showing rates obtained from time-dependent calculations of ground-state H_2^+ in a low-frequency external field (peak intensity $I = 10^{14} \text{ W cm}^{-2}$, $\lambda = 1064 \text{ nm}$) rising linearly over five cycles. The ionization rates were then obtained from the exponential decay of the electron density. The results show maxima at $R \sim 7 a_0$ and $R \sim 10 a_0$, and rates of about $(1\text{--}8) \times 10^{-3} \text{ fs}^{-1}$. These values of the ionization rates (Zuo and Bandrauk 1995b) are much lower than our static field results (figure 1(c)) for $F \geq 0.04 \text{ au}$. However, their peaks correspond very well to our time-averaged results for $F = 0.045 \text{ au}$ (table 2 and figure 6). While the first peak (near $R \sim 7 a_0$) has about the same magnitude, our second peak is much stronger: this may be partly due to their method of calculation which confines the wavefunction within a cylinder aligned along the z -axis and may not allow for full three-dimensional spreading to occur. Apart from this feature the two sets of results agree

Table 1. Time-averaged ionization rates $\bar{\Gamma}$ (fs^{-1}).

R (a_0)	$F_0 = 0.053\,38$ au		$F_0 = 0.08$ au	
	g rate	u rate	g rate	u rate
2.0		0.156E-2	0.830E-7	0.182E+0
2.5		0.767E-3	0.508E-5	0.143E+0
3.0	0.110E-7	0.803E-3	0.796E-4	0.160E+0
3.5	0.178E-6	0.139E-2	0.459E-3	0.200E+0
4.0	0.133E-5	0.311E-2	0.139E-2	0.217E+0
4.5	0.512E-5	0.726E-2	0.288E-2	0.192E+0
5.0	0.132E-4	0.149E-1	0.487E-2	0.150E+0
5.5	0.267E-4	0.223E-1	0.710E-2	0.127E+0
6.0	0.456E-4	0.230E-1	0.942E-2	0.132E+0
6.5	0.712E-4	0.194E-1	0.123E-1	0.227E+0
7.0	0.102E-3	0.147E-1	0.147E-1	0.456E+0
7.5	0.134E-3	0.125E-1	0.164E-1	0.460E+0
8.0	0.171E-3	0.164E-1	0.186E-1	0.327E+0
8.5	0.218E-3	0.286E-1	0.221E-1	0.224E+0
9.0	0.266E-3	0.486E-1	0.253E-1	0.189E+0
9.5	0.301E-3	0.477E-1	0.261E-1	0.207E+0
10.0	0.329E-3	0.339E-1	0.254E-1	0.109E+0
10.5	0.367E-3	0.220E-1	0.256E-1	0.158E+0
11.0	0.428E-3	0.165E-1	0.279E-1	0.135E+0
11.5	0.505E-3	0.119E-1	0.327E-1	0.110E+0
12.0	0.568E-3	0.762E-2	0.384E-1	0.142E+0
12.5	0.588E-3	0.614E-2	0.410E-1	0.106E+0
13.0	0.578E-3	0.841E-2	0.389E-1	0.755E-1
13.5	0.565E-3	0.731E-2	0.350E-1	0.113E+0
14.0	0.572E-3	0.568E-2	0.317E-1	0.103E+0

well for $R > 5 a_0$. For $R \leq 5 a_0$ the results of Zuo and Bandrauk (1995b) are higher and correspond to our time-averaged results for higher fields up to $F = 0.053\,38$ au as R decreases. The comparison suggests that the bulk of the ionization by the dynamic field takes place near the end of the ramping period before the field envelope has reached its maximum. For small R , the initial g-state is tightly bound and ionization will mainly occur during the plateau of the field.

The positions of the peaks in figure 1 of Zuo and Bandrauk (1995b) allow us to make the above suggestion. The fact that the amplitudes are generally comparable is intriguing as it would suggest that a very large fraction of the wavefunction is mixed into the u-state at any given moment. It should be pointed out that the mixing of u- and g-states does not necessitate multiphoton promotion of the electron (Chelkowski and Bandrauk 1995) at larger internuclear distances. The reason is that the localized electronic wavefunction does not change adiabatically as the field oscillates. At each moment we have a superposition of the g- and u-states, of which the u-component is readily ionized as the field reaches its maximum. However, during the following half-cycle the field changes sign and the ‘old’ g-state component of the wavefunction becomes the ‘new’ u-state component and continues to ionize at the appropriate rate. In other terms, the localized, stable downhill well becomes the localized, unstable uphill well in rhythm with the optical frequency. The strong g–u conversion (Rabi flopping) and low laser frequency justify the comparison (figure 6) of the u-state time-averaged results (tables 1 and 2) with the time-dependent AC ionization rate from the ground state (Zuo and Bandrauk 1995b).

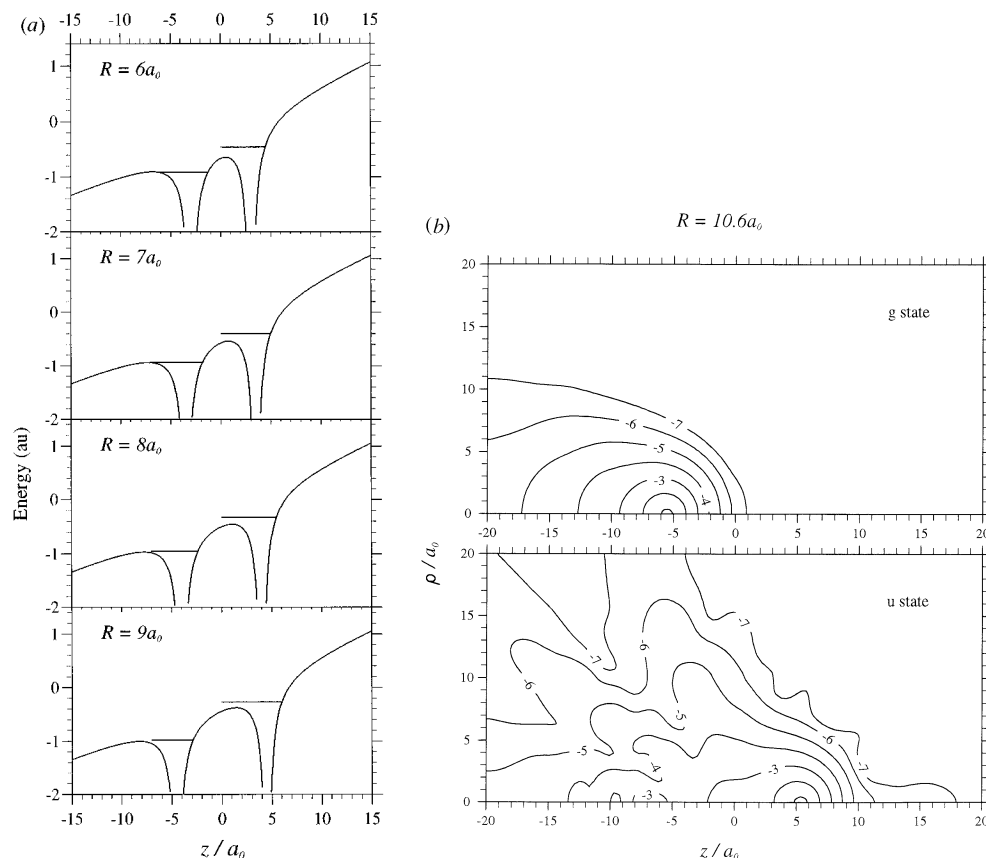
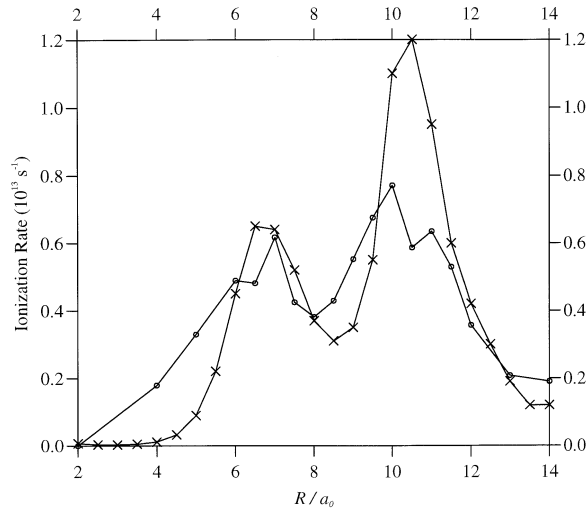


Figure 5. (a) The electronic potential along the internuclear axis for $F = 0.08$ au. The real parts of the u- and g-quasienergies are indicated in the figures. (b) Contour plots of the logarithm to base 10 of $|\Psi|^2$ at field strength $F = 0.08$ au at $R = 10.6a_0$. Contours are at intervals of powers of 10, down to a minimum power -8 .

Furthermore, the process of dissociative ionization may not require stepwise multiphoton excitation but can occur through the dynamics of the dressed states. The strong deformation of the g-well due to the laser (figure 1) can lead to strong nonadiabatic *vibrational* excitation leading to dissociation. For values of R greater than several a_0 the u-g conversion can occur as outlined above. The degree of this mixing would depend on the dissociation speed and should be sensitive to the nuclear masses, and thus would show isotope dependence. The stepwise multiphoton process would not show such sensitivity, and this should permit one to distinguish between the mechanisms. Moreover, this type of well deformation, were it to occur, would imply a broad spread of fragment ion energies with little evidence of vibrational structure. As long as the dissociation time is slow on the optical timescale, mixing of upper and lower states will occur. In practice, this condition is commonly satisfied in experiments involving heavy molecules in low-frequency fields (Codling and Frasinski 1993).

Table 2. Time-averaged ionization rates $\bar{\Gamma}$ (fs^{-1})

R (a_0)	$F_0 = 0.04$ au		$F_0 = 0.045$ au		$F_0 = 0.05$ au		$F_0 = 0.06$ au	
	g rate	u rate	g rate	u rate	g rate	u rate	g rate	u rate
2.0		0.56E-5		0.71E-4		0.52E-3		0.88E-2
2.5		0.18E-5		0.27E-4		0.23E-3		0.51E-2
3.0		0.16E-5		0.26E-4		0.24E-3	0.19E-6	0.56E-2
3.5		0.28E-5		0.46E-4	0.32E-7	0.41E-3	0.26E-5	0.93E-2
4.0		0.73E-5	0.22E-7	0.11E-3	0.31E-6	0.96E-3	0.14E-4	0.18E-1
4.5	0.56E-8	0.23E-4	0.12E-6	0.32E-3	0.13E-5	0.25E-2	0.44E-4	0.34E-1
5.0	0.22E-7	0.71E-4	0.40E-6	0.89E-3	0.37E-5	0.59E-2	0.10E-3	0.47E-1
5.5	0.65E-7	0.20E-3	0.97E-6	0.22E-2	0.81E-5	0.11E-1	0.18E-3	0.47E-1
6.0	0.15E-6	0.52E-3	0.19E-5	0.45E-2	0.15E-4	0.15E-1	0.29E-3	0.39E-1
6.5	0.28E-6	0.11E-2	0.33E-5	0.65E-2	0.23E-4	0.14E-1	0.42E-3	0.31E-1
7.0	0.46E-6	0.20E-2	0.52E-5	0.64E-2	0.35E-4	0.11E-1	0.55E-3	0.28E-1
7.5	0.72E-6	0.23E-2	0.76E-5	0.52E-2	0.48E-4	0.83E-2	0.71E-3	0.41E-1
8.0	0.11E-5	0.20E-2	0.10E-4	0.37E-2	0.62E-4	0.78E-2	0.91E-3	0.78E-1
8.5	0.15E-5	0.14E-2	0.13E-4	0.31E-2	0.79E-4	0.11E-1	0.11E-2	0.11E+0
9.0	0.19E-5	0.11E-2	0.17E-4	0.35E-2	0.99E-4	0.20E-1	0.12E-2	0.96E-1
9.5	0.23E-5	0.91E-3	0.21E-4	0.55E-2	0.12E-3	0.30E-1	0.13E-2	0.64E-1
10.0	0.29E-5	0.98E-3	0.26E-4	0.11E-1	0.13E-3	0.28E-1	0.15E-2	0.44E-1
10.5	0.36E-5	0.17E-2	0.30E-4	0.12E-1	0.15E-3	0.19E-1	0.18E-2	0.35E-1
11.0	0.43E-5	0.32E-2	0.33E-4	0.95E-2	0.16E-3	0.13E-1	0.21E-2	0.24E-1
11.5	0.49E-5	0.37E-2	0.35E-4	0.60E-2	0.19E-3	0.94E-2	0.21E-2	0.17E-1
12.0	0.53E-5	0.28E-2	0.39E-4	0.42E-2	0.22E-3	0.64E-2	0.21E-2	0.20E-1
12.5	0.57E-5	0.17E-2	0.46E-4	0.30E-2	0.25E-3	0.41E-2	0.21E-2	0.23E-1
13.0	0.63E-5	0.12E-2	0.54E-4	0.19E-2	0.27E-3	0.33E-2	0.21E-2	0.17E-1
13.5	0.72E-5	0.84E-3	0.61E-4	0.12E-2	0.26E-3	0.45E-2	0.23E-2	0.17E-1
14.0	0.84E-5	0.50E-3	0.65E-4	0.12E-2	0.26E-3	0.38E-2	0.27E-2	0.21E-1

**Figure 6.** The ionization rate of H_2^+ : a comparison between the time-dependent results of Zuo and Bandrauk (1995b, figure 1, \circ) and our time-averaged DC results for $F_0 = 0.045$ au (table 2, \times).

4. Conclusions

Barrier models of electron release have been used successfully for many years. Their use is particularly well known in the collisions of multiply charged ions with atoms: an example

of their utility is provided by the Bohr–Lindhard model of electron capture (Bransden and McDowell 1993). However, our results show that the one-dimensional potential barrier model cannot explain the variation in ionization rate with respect to R and F for the simple system H_2^+ . The reflected and transmitted wavefunctions from the three-dimensional potential barriers are more complex than the model allows for. The more complicated situations require a full quantum-mechanical treatment: perhaps in terms of scattering by the second nucleus with distortions due to the presence of the field. This scattering interpretation is investigated in a one-dimensional quantum well model by McCann and Plummer (1996). Semiclassical models, if applicable, would need to allow for the possibility of the electron escaping from the upper well and moving around the lower well to escape at an angle. In summary, the classical barrier model is reasonable, but tunnelling, diffraction and over-barrier reflection are quantal effects and one should not expect the classical model to yield accurate quantitative results. While quantal effects are less important for the rims of deep potential wells (Bransden and McDowell 1993), which correspond to short de Broglie wavelengths, more detailed theoretical work is required to resolve this issue conclusively.

Our results indicate that, for antibonding orbitals, tunnelling ionization is greatly enhanced at intermediate internuclear separation for strong fields. This critical range is rather far from the equilibrium separation of the molecule for moderate fields. It may be argued that in dissociative ionization the bulk of the ionization will take place at the inner maximum (figure 1(c)) and thus the potential barrier model will work well. This may well be the case for the experimental Coulomb explosions for which R_D is not substantially larger than R_E . However, for higher fields with maxima shifting to smaller R the more complicated ionization mechanism may be important. In the many-electron cases described in section 1 the potential barrier model gives good order of magnitude agreement with experiment. The current calculations suggest that to improve on this agreement will require sophisticated calculations beyond the intuitive nature of the potential barrier model. Detailed many-body time-dependent calculations might be required to test whether this process is a general feature of dissociative ionization.

Theoretically, the quasistatic field is a very useful model of the low-frequency dynamic field, showing how ionization is likely to vary as the molecule dissociates. We are currently in the process of extending our AC calculations (see I) to low-frequency (for example, 1064 nm) laser fields, to compare results. Finally, we note that, as with the work discussed in section 1, the current calculations again show strongly enhanced ionization at particular values of R . Remembering that Chelkowski *et al* (1995) find that including ionization channels impedes stabilization of the molecule, our results seem to give added weight to the ‘ionization’ interpretation of the Coulomb explosion experiments. However, our DC work is mainly applicable to low-frequency AC situations for which stabilization may not be possible to begin with (Plummer and McCann 1995a). Our comparison with Zuo and Bandrauk (1995b) suggests that the ionization tends to take place near the beginning of the pulse. We note that very recent experimental results for I_2 (Normand and Schmidt 1996) seem to demonstrate stabilization: Normand and Schmidt require certain of the molecular ions to delay their fragmentation in the presence of the laser pulse to explain their results. However, also very recently, Posthumus *et al* (1996), considering I_2 experimentally and with barrier-model calculations, claim that stabilization is unnecessary. Detection of molecular ions at or near the end of the pulse would seem to be the best method experimentally to distinguish between the two mechanisms.

Acknowledgments

Calculations were carried out on the University of Durham IT Service cluster and the Atomic and Molecular Physics (ATMOL) cluster. We would like to thank Drs K Codling, J Posthumus, L J Frasinski and R M Potvliege for helpful discussions and Dr E L Heck for assistance with the computing facilities. This research was funded by the Engineering and Physical Sciences Research Council and the Computational Science Initiative.

References

- Brandsen B H and McDowell M R C 1993 *Charge Exchange and the Theory of Ion-Atom Collisions* (Oxford: Oxford University Press) ch 1
- Broad J T 1982 *Phys. Rev. A* **26** 3078
- Codling K and Frasinski L J 1993 *J. Phys. B: At. Mol. Opt. Phys.* **26** 783
- Chelkowski S and Bandrauk A D 1995 *J. Phys. B: At. Mol. Opt. Phys.* **28** L723
- Chelkowski S, Zuo T, Atabek O and Bandrauk A D 1995 *Phys. Rev. A* **52** 2977
- Dörr M, Potvliege R M and Shakeshaft R 1990 *Phys. Rev. Lett.* **64** 2003
- Giusti-Suzor A, Mies F H, DiMauro L F, Charron E and Yang B 1995 *J. Phys. B: At. Mol. Opt. Phys.* **28** 309
- Ivanov M V 1995 *19th ICPEAC* ed J B A Mitchell, J W McConkey and C E Brion Abstracts p 740
- McCann J F and Plummer M 1996 *J. Phys. B: At. Mol. Opt. Phys.* to be submitted
- Maquet A, Chu S-I and Reinhardt W P 1983 *Phys. Rev. A* **27** 2946
- Normand D and Schmidt M 1996 *Phys. Rev. A* **53** R1958
- Piroux B and Shakeshaft R 1994 *Phys. Rev. A* **49** 3903
- Plummer M and McCann J F 1995a *J. Phys. B: At. Mol. Opt. Phys.* **28** L119
- 1995b *J. Phys. B: At. Mol. Opt. Phys.* **28** 4073
- Posthumus J H, Frasinski L J, Giles A J and Codling K 1995 *J. Phys. B: At. Mol. Opt. Phys.* **28** L349
- Posthumus J H, Giles A J, Thompson M R, Shaikh W, Langley A J, Frasinski L J and Codling K 1996 *J. Phys. B: At. Mol. Opt. Phys.* **29** L525
- Potvliege R M and Shakeshaft R 1989 *Phys. Rev. A* **40** 3061
- Reinhardt W P 1979 *Comput. Phys. Commun.* **17** 1
- Schmidt M, Normand D and Cornaggia C 1994 *Phys. Rev. A* **50** 5037
- Seideman T, Ivanov M Yu and Corkum P B 1995 *Phys. Rev. Lett.* **75** 2819
- Watson D K 1986 *Phys. Rev. A* **34** 1016
- Zuo T and Bandrauk A D 1995a *Phys. Rev. A* **51** R26
- 1995b *Phys. Rev. A* **52** R2511